

On the stiction of MEMS materials

Y.X. Zhuang and A. Menon*

MIC, Department of Micro and Nanotechnology, Technical University of Denmark, Building 345 east, DK-2800, Kgs. Lyngby, Denmark

Received 19 September 2004; accepted 27 February 2005

Stiction is a serious problem in microelectromechanical systems (MEMS) due to their large surface area-to-volume ratio. Stiction is closely related to surface forces, which greatly depend on the materials used, surface topography and surface treatment process. In this paper, we investigate surface energies and stiction of commonly used MEMS materials by contact angle measurements and atomic force microscopy (AFM). Dispersive and polar components of surface energies are calculated by Owens–Wendt–Rabel–Kaelble method. Silicon and silicon-related materials have higher polar surface energies than SU-8 and polymethylmethacrylate (PMMA), thereby have larger surface energies and enhanced tendency for stiction. The nano-scale adhesion forces between Si_3N_4 tip and surfaces obtained by AFM further verified that silicon wafer with native oxide has 3–4 times higher adhesion force than SU-8 and PMMA. It has been shown that the materials with higher surface energy have higher stiction/adhesion forces. The topography of surface influences the contact angle and stiction, and is also discussed in the paper.

KEY WORDS: stiction, contact angle, surface energy, adhesion/stiction forces, roughness, MEMS materials

1. Introduction

The materials widely used in microelectromechanical systems (MEMS) are silicon and silicon-related materials, polymer, glass and ceramics [1]. Silicon and silicon-related materials are still widely used in MEMS due to their mature fabrication technologies and unique properties. However, silicon and silicon-related materials are not the only materials used in the design and manufacture of MEMS devices. Polymers have become increasingly popular in fabricating MEMS devices, and have been widely used as photoresist, stamps for hot embossing and imprinting, conductors and insulators, and for protective coatings. Polymers are paving the way in bio-MEMS, microfluidic devices, and various sensors due to their low cost, biocompatibility, good machining ability, high corrosion resistance, and high flexibility in structures and properties. Among various polymers, SU-8 and poly-methylmethacrylate (PMMA) are the most commonly used. SU-8, a negative, epoxy-based near-UV photoresist, is a fascinating material for microfabrication combining the processing of ultra-thick resist layers and outstanding lithographic performance [2], and has found increased applications in microfluidic channels, stamps for hot embossing, moulds for electroplating, materials for cantilever, sensors and waveguides, and other applications. The PMMA molecule is a polymer chain made of polymerized methylmethacrylate. PMMA as well as SU-8 are the widely used materials for microfluidic and microoptical systems.

In microsystems, due to large surface area-to-volume ratio, surface forces become dominant forces and play a

relatively large role compared to gravity and inertia. This results in large surface adhesion and stiction since the restoring force cannot overcome the attractive interfacial forces caused by capillary, van der Waals, and electrostatic forces [3,4]. The stiction can occur during fabrication (release stiction) and/or in applications (in-use stiction). The surface adhesion and stiction strongly affect the reliability and long-term durability of MEMS devices, and become a serious problem in fabrication and application of MEMS devices. The mechanisms of adhesion and stiction have been widely investigated [3,4]. It has been found that surface adhesion and stiction is closely related to the surface energy of solid and surface topography. Capillary induced stiction is important for both release stiction and in-use stiction. Special drying processes such as CO_2 drying can eliminate release stiction in some situations. However, in some processes and applications, this is not feasible. In-use stiction related failures is a major problem and will be increasingly important with miniaturization towards nano-scale structures. Hydrophobization of surfaces to decrease surface energy is the primary technique used to minimize stiction related problems. Both liquid-based and vapour-based processes are investigated in this regard. In order to avoid stiction in MEMS devices, it is quite important to use suitable materials/processes or give proper surface modifications for various MEMS devices and applications. Therefore, it was decided to investigate the surface energies of various common materials used in MEMS, which could give a general idea about materials selection, and the methods to avoid stiction. In this paper, the commonly used materials in MEMS, such as silicon, poly silicon, silicon nitride, SU-8 and PMMA, are studied and discussed in

*To whom correspondence should be addressed.
E-mail: am@mic.dtu.dk

terms of wettability, surface energy, roughness, nano-scale adhesion forces and ranked based on their susceptibility for stiction. The effect of surface modification, coating and surface texturing on the contact angle has also been discussed.

2. Theory of surface energy

The surface energy is very important in view of adhesion, packaging, and reliability of MEMS devices. Surface energy is related to the contact angle of liquid on the surface by the Young's equation [5].

$$\gamma_{sv} = \gamma_{sl} + \gamma_{lv} \cos \theta \quad (1)$$

where γ_{sv} , γ_{sl} , and γ_{lv} are surface energy of solid, interfacial tension between solid and liquid, and surface tension of liquid, respectively. θ is the equilibrium contact angle of liquid on the solid surface. In order to get the surface energy from the contact angle measurements, it is necessary to know the relationship of γ_{sl} with γ_{sv} and γ_{lv} . Up to now, there are many assumptions for this relationship. In this paper, we use Owens–Wendt–Rabel–Kaelble method [6–8] to evaluate the surface energy of various solid surfaces. In this method, the surface tension of each phase can be split into a polar and a dispersive fraction, i.e.

$$\gamma_{sv} = \gamma_{sv}^D + \gamma_{sv}^P, \text{ and } \gamma_{lv} = \gamma_{lv}^D + \gamma_{lv}^P \quad (2)$$

The interfacial tension γ_{sl} can be calculated by the geometric mean equation,

$$\gamma_{sl} = \gamma_{sv} + \gamma_{lv} - 2 \left(\sqrt{\gamma_{sv}^D \gamma_{lv}^D} + \sqrt{\gamma_{sv}^P \gamma_{lv}^P} \right) \quad (3)$$

where superscripts D and P represent the dispersive and polar components, the subscripts s, l, v denote solid, liquid and vapour phases, respectively. Combining equation (3) with Young's equation (1), the following linear equation can be obtained,

$$\frac{(1 + \cos \theta) \gamma_{lv}}{2 \sqrt{\gamma_{lv}^D}} = \sqrt{\gamma_{sv}^P} \sqrt{\frac{\gamma_{lv}^P}{\gamma_{lv}^D}} + \sqrt{\gamma_{sv}^D} \quad (4)$$

Therefore, with at least two liquids with known values γ_{lv} , γ_{lv}^D , and γ_{lv}^P , the components of γ_{sv}^D and γ_{sv}^P can be determined from the intercept and the slope of the linear fit to the data. The total surface energy of solid can be calculated by summing the two parts.

3. Experimental techniques

3.1. Materials preparation

All the materials investigated in this paper have *n*-(100) blank silicon wafer as starting material. The

fabrication of the sample relies on the standard clean-room process. The process sequences for various materials are given in figure 1. The measurements were carried out at the steps marked with *. Among silicon and silicon compounds, silicon, undoped poly-silicon, and low stress silicon nitride have been chosen for this investigation. The 0.3 μm thick un-doped ploy silicon was grown on silicon substrate by silane decomposition at 620 $^\circ\text{C}$ using low-pressure chemical vapour deposition (LPCVD) techniques. The 0.3 μm thick low stress silicon nitride was deposited on silicon substrate by plasma enhanced chemical vapour deposition (PECVD) technique using standard recipe for low stress silicon nitride. In silicon surface micromachining, hydrofluoric (HF) acid is used to remove silicon oxide sacrificial layer. To simulate the process, the *n*-(100) silicon wafer, undoped poly silicon, and silicon nitride are also given a buffered HF (BHF) dip for 30 s, followed by 5 min rinse in DI water and spin dry afterwards. Stiction is a common problem for surface micromachining due to high surface energy of silicon and silicon related materials. Therefore, fluorocarbon film, which is a Teflon-like film and can be used as anti-stiction layer in MEMS devices, is deposited on silicon substrate by passivation process in deep reactive ion etching (DRIE), where C_4F_8 is used as feed gas. After feeding C_4F_8 into the DRIE chamber, the C_4F_8 gas are ionized between the anode and cathode to form ion or radicals such as CF_2 , CF_3 , CF , etc., the radicals diffuse to the substrate and polymerize to form a fluorocarbon (C_xF_y)_z film.

As described in figure 1(b), 2 μm thick PMMA layer was prepared on the *n*-(100) silicon wafer. After giving silicon substrate a BHF dip for 30 s, followed by 5 min rinse in water and spin dry, PMMA solution was spun on the fresh pre-treated silicon substrate and post-baked at 150 $^\circ\text{C}$ for 5 min to remove solvent. Then PMMA is ready for measurements.

Five micrometer thick SU-8 layer [9] was prepared by a normal process as given in figure 1(c) with the following steps: substrate pre-treatment, spin coat, soft bake to evaporate the solvent and densify the film, UV exposure without mask to complete cross-linking, post exposure bake to accelerate the cross-linking, develop in propyleneglycol monomethylether acetate (PGMEA), rinsed with isopropanol (IPA), and dry.

3.2. Surface characterization techniques

Contact angle measurements were performed using contact angle meter DSA10 from Krüss GmbH equipped with automatic dispensing system and Framegrabber. The contact angles were determined by drop shape analysis software. Test liquids were deionised (DI) water, diiodomethane (Aldrich 99%), and Ethylene Glycol (Aldrich 99.8%) due to their wide range of surface tension and ratio of dispersive to polar component.

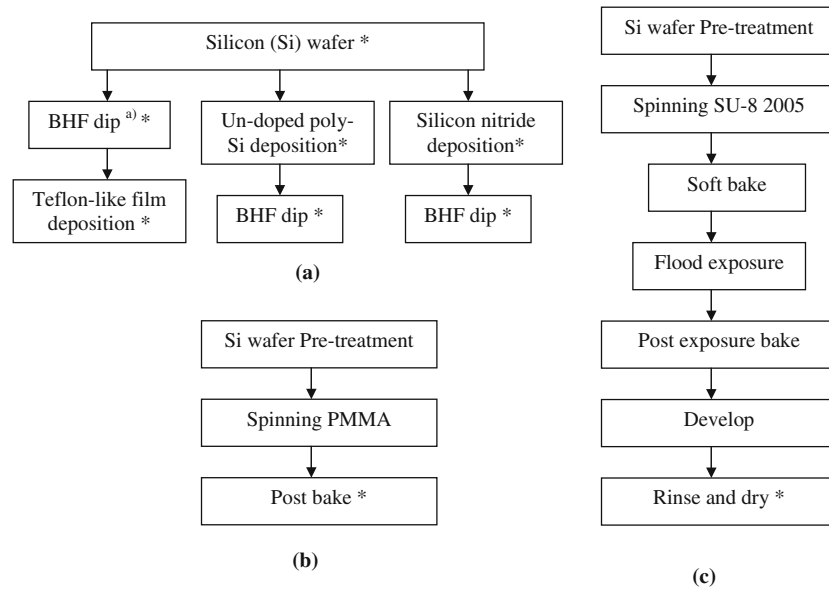


Figure 1. Process sequences for silicon and silicon-related materials (a), PMMA (b), and SU-8 (c). Measurements have been performed after the processes marked *. (a) BHF dip is a process to simulate etching of sacrificial layer, which is dipped into buffered HF for 30 s, followed by 5 min rinse in water and spin dry.

No stick/slip and swelling phenomena have been observed during static and dynamic contact angle measurements. The surface tensions of the three liquids [10] are given in table 1. Both static and dynamic contact angles have been measured. For static contact angles, the contact angle values were taken 5 s after depositing the drops on the surface to allow drops relaxation. At least 10 measurements have been performed for each droplet. The accuracy of measurement is $\pm 0.5^\circ$. The static contact angle values reported are the average of at least three droplets. The advancing and receding contact angles were measured with pumping liquid steadily into the sessile drop or withdrawing it using a motor-driven syringe. A $2 \mu\text{L}$ initial sessile droplet was first deposited on the surface, after 10 s relaxation time, the test liquid is steadily pumped into the initial sessile droplet until base diameter of the droplet is larger than 6.5 mm, and then the liquid is steadily sucked from the droplet into the needle using a motor-driven syringe. The contact angles were calculated and recorded around every second during the experiments. In order to eliminate the effect of dispensing needle, the advancing and receding contact angles are the average values for the drops, whose base diameters are six times larger than diameter of the dispensing needle.

A typical dynamic contact angle curve as a function of time is given in figure 2 together with the base diameter of liquid droplet. The dynamic contact angle curve can be divided into four regions as separated by line A, B and C. With steadily pumping the test liquid into the initial droplet, the dynamic contact angle keeps constant, and the base diameter increases. The advancing contact angle can be determined from the average value in this region. At point A, the liquid starts to be withdrawn into the syringe, the

base diameter of the droplet keeps constant even though the volume of the liquid droplet decreases with the time. In this region (between point A and point B), the dynamic contact angle decreases with the time. This region can be regarded as a transition region. From point B, the base diameter of the droplet decreases together with the volume of the droplet, while the dynamic contact angle nearly keeps constant, which can be considered as the receding contact angle. From point C, the contact angle decreases quickly with the time; the needle might have influence on the receding contact angle due to small base diameter.

The surface roughness has been measured by atomic force microscopy (AFM) in contact mode using commercial silicon tips. Nano-scale adhesion tests were carried out with a commercial AFM system (Dimension 3100 Scanning Probe Microscope, Digital Instrument) operating under ambient conditions of 22°C and 45–50% RH. Square pyramidal Si_3N_4 tips with a nominal 20–60 nm radius mounted on gold-coated Si_3N_4 cantilevers with a nominal spring constant of 0.32 N/m (Digital Instrument) were used in this study. The adhesion force measurements were carried out in force calibration mode. During the force calibration mode, a force distance curve is obtained by exciting the PZT in the Z direction with a saw tooth wave force. The adhesion forces can be determined from the force distance curves [11,12].

4. Results and discussions

4.1. As-deposited and as-received materials

The nature of materials is quite important in determining contact angles and surface energies. As a starting

Table 1.
Surface tension of three test liquids [10].

Test liquids	Total surface energy (mN/m)	Dispersive component (mN/m)	Polar component (mN/m)
DI-water	72.8	21.8	51
Diiodomethane	50.8	50.8	0
Ethylene glycol	47.7	30.9	16.8

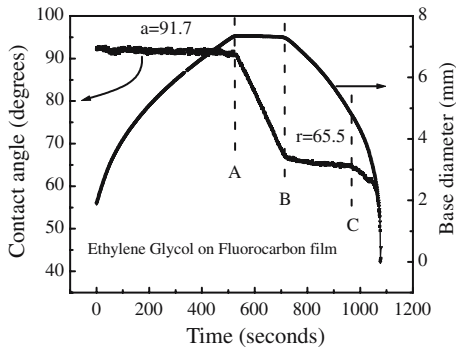


Figure 2. Dynamic contact angle of ethylene glycol on fluorocarbon film and base diameter of the droplet as a function of time.

point, the investigation for as-received and as-deposited materials could give us a general idea about surface energies and materials properties. The water contact angles and surface energies of *n*-(100) silicon, undoped poly silicon, low stress silicon nitride, PMMA and SU-8 are given in figure 3. It can be seen that the silicon and silicon-related materials have smaller water contact angles and thereby larger surface energies than PMMA and SU-8, indicating that the silicon and silicon-related materials are intended to stick together in fabrication and application, while PMMA and SU-8 can be regarded as hydrophobic surface due to relative low surface energy, and have fewer tendencies for stiction. The inset in figure 3 gives root mean square (RMS) roughness of the as-deposited materials, which is calculated from the AFM images with $5 \times 5 \mu\text{m}^2$ area.

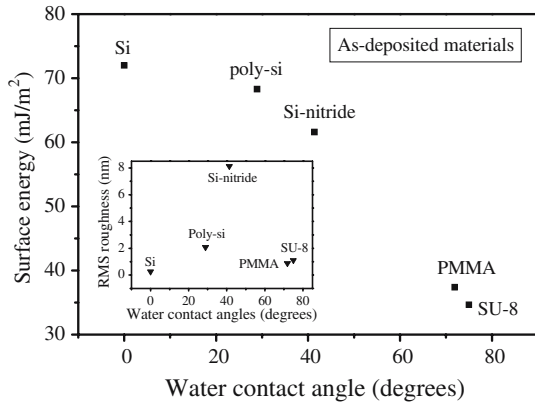


Figure 3. Surface energy and static water contact angle of as-received and as-deposited MEMS materials. The inset shows the root mean square (RMS) roughness and static water contact angle of the MEMS materials.

Although PMMA and SU-8 have similar RMS roughness as silicon, they have larger water contact angles due to the nature of materials.

The contact angles of DI water, diiodomethane and ethylene glycol on the five as-received and as-deposited MEMS materials are displayed in figure 4(a). It can be observed that water and ethylene glycol contact angles vary a lot from silicon-related materials to polymer PMMA and SU-8, while there is little change for diiodomethane contact angles. As shown in table 1, diiodomethane is a dispersive liquid, while water and ethylene glycol are polar liquids. This might indicate that the five as-deposited materials have similar values of dispersive surface energy, while the polar component of surface energy decreases from silicon to PMMA and SU-8. The total surface energy and its dispersive and polar components are calculated from the advancing contact angles using Owens–Wendt–Rabel–Kaelble method as described above, and given in figure 4(b). It can be clearly seen that the dispersive component of

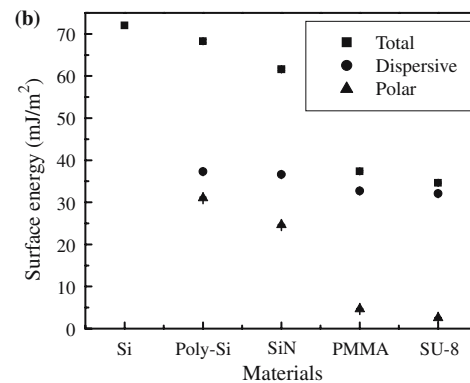
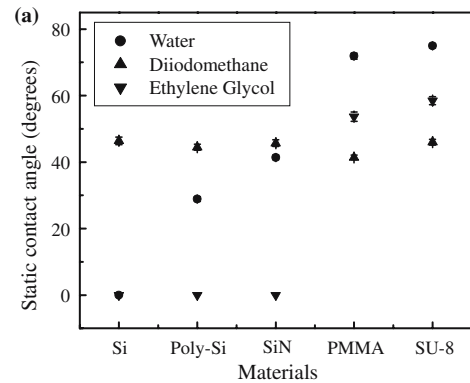


Figure 4. Static contact angles of various test liquids on the as-received and as-deposited MEMS materials (a), and surface energy of the MEMS materials (b).

surface energy does not change too much for the five as-deposited materials, while the total surface energy decreased a lot from silicon to PMMA and SU-8 due to lower polar component. It can be concluded that PMMA and SU-8 have lower surface energies than silicon wafer due to lower value of polar surface energy, and therefore lower tendency for stiction, which has been further verified by the nano-scale adhesion force measurements (see results below).

Stiction is a serious problem in MEMS devices fabrication and application, which is mainly caused by capillary force, van der Waals force, and electrostatic force. The in-use capillary force, F_{cap} , is caused by capillary condensation and can be calculated as [4]

$$F_{\text{cap}}(d) = \frac{4\gamma_{\text{lv}}r_{\text{k}}(\cos\theta)^2}{d^2} \quad (5)$$

where γ_{lv} is surface tension of water, θ is the contact angle on the surface and assumed same values for both surfaces, d is the separation distance between the two surfaces, r_{k} is the Kelvin radius and given by Kelvin equation, and has value around -0.78 nm at 50% relative humidity [4]. The attractive capillary force decreases with increasing water contact angle. Assuming d is $1 \mu\text{m}$, the attractive capillary force for poly-silicon is $2.32 \mu\text{N}/\mu\text{m}^2$, while $0.36 \mu\text{N}/\mu\text{m}^2$ for SU-8, 6.5 times lower than that of poly-silicon. This further proves that SU-8 and PMMA might have lower probability to stick. What are considered here are two perfect and smooth surfaces. In practical cases, most micro-machined surfaces are rough. The contact angle might change from one process to another since the contact angles depend also on the roughness of the surfaces.

4.2. Surface modifications

As stated above, the contact angles can be changed by various techniques. Although silicon and silicon-related materials have serious stiction problems, they are still widely used in MEMS devices due to their desirable mechanical properties. Hence, in order to avoid stiction, surface modifications or coatings are commonly used in silicon microstructures fabrication. During surface micromachining, oxide sacrificial layer is normally etched away in HF solution, which changes surface state and leaves an H-terminated surface. The H-termination is believed to improve hydrophobization of the surfaces. Figure 5 gives the water contact angles and surface energies of as-deposited and buffered HF (BHF) dipped silicon, poly-silicon, and silicon nitride. It can be observed that the BHF dips increase hydrophobization of silicon and poly-silicon surfaces. However, for silicon nitride, the BHF dip does not improve the hydrophobization of the surface. The H-terminated surface has lower surface energy compared to bare silicon, but in

some case, it is still not enough to avoid stiction. On the other hand, the H-terminated surface is not stable enough for anti-stiction application due to re-oxidization in air. The hydrocarbon or fluorocarbon films with low surface energy can be deposited on the surfaces to change the high surface energy to low surface energy surface [13]. Fluorocarbon film deposited by passivation process in DRIE tool is a very convenient process to avoid stiction. The static contact angle of DI water, diiodomethane, and ethylene glycol on fluorocarbon film is 110° , 88.5° , and 86.6° , respectively. The total surface energy is calculated to be as low as $14.32 \text{ mJ}/\text{m}^2$ as shown in figure 5(b), in which the dispersive component is 14.09 and polar component is $0.24 \text{ mJ}/\text{m}^2$. The deposition of fluorocarbon film is an efficient way to avoid in-use stiction. It has been reported that the water contact angle can be as high as 130° if fluorocarbon film is roughed by varying the deposition parameters [14].

Nano-scale adhesion forces between Si_3N_4 AFM tip and surfaces have been measured and shown in figure 6. The adhesion forces of SU-8 and PMMA are 3–4 times smaller than that of as-received silicon wafer, which has a native oxide layer, indicating that SU-8 and PMMA have smaller tendency for stiction, which is in agreement with the conclusion above. The BHF dip can dramatically decrease the adhesion force of silicon wafer since it produces an H-terminated surface. Among all the materials investigated, the fluorocarbon film deposited by DRIE has smallest adhesion force, which is 33 nN , 4.7 times smaller than that of as-received silicon wafer. Therefore, the fluorocarbon films are quite adequate for most applications. Figure 7 shows the nano-scale adhesion force versus the total surface energy of some MEMS materials. It has been shown that the materials with higher surface energies have higher adhesion forces, and thereby higher tendency for stiction.

4.3. Influence of roughness

It is well known that the contact angles and wettability of a surface is also a function of its roughness. It has been commonly realized that by microtexturing a surface to increase its roughness, the apparent contact angle can be increased in the hydrophobic case, while decreased in the hydrophilic case. The phenomenon can be explained by Wenzel's approach, where it is assumed that the contact between solid and liquid is maintained at every point, i.e. complete contact. If the roughness is not very great, for the wetted surface, the apparent contact angle for rough surface can be expressed by Wenzel's approach [15]

$$\cos\theta_r = r \cos\theta_0 \quad (6)$$

where r is the ratio of the actual area of liquid–solid contact to the projected area on the horizontal plane,

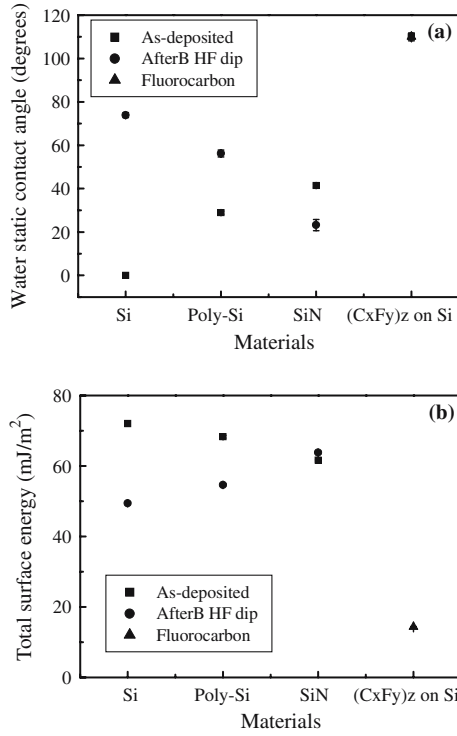


Figure 5. Static water contact angle (a) and surface energy (b) of the silicon-related materials before and after BHF dip and fluorocarbon films.

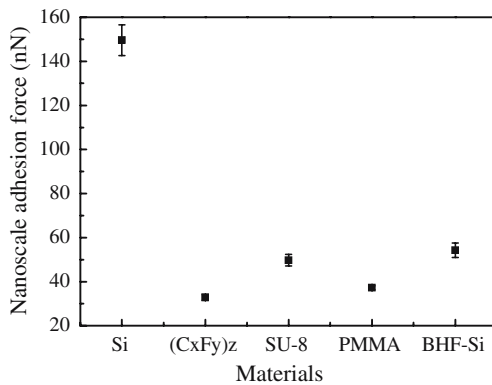


Figure 6. Nano-scale adhesion forces between Si_3N_4 tip and surfaces for some MEMS materials.

and larger than 1. θ_r is the contact angle of rough surface, and θ_0 is the equilibrium contact angle of the liquid drop on smooth surface. On the other hand, if the contact angle is larger than 90° (i.e. hydrophobic surface), and the surface rough enough, the liquid may trap air so that a composite surface is formed, and the apparent contact angle of rough surface can be expressed by Cassie's equation [16]

$$\cos \theta_r = f_1 \cos \theta_0 - f_2 \quad (7)$$

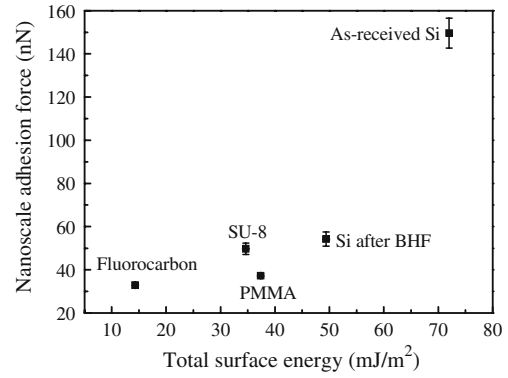


Figure 7. Relationship between nano-scale adhesion forces and surface energies.

in which f_1 is the wetted surface area fraction, and f_2 is the unwetted surface area fraction, and $f_1 + f_2 = 1$.

The effect of roughness on the contact angle depends on the properties of materials and the details of the topography. Silicon and silicon-related materials have $\theta_0 < 90^\circ$, according to Wenzel's equation, the apparent water contact angle of silicon and silicon-related materials decreases with increased roughness, thereby the attractive capillary force increases. However, with the roughness increasing, the van der Waals force F_{vdw} between two proximity surfaces decrease due to reduced real contact area according to the equation [17],

$$F_{vdw} = -\frac{HA}{6\pi d^3} \quad (8)$$

where H is the Hamaker constant, A is the shared area of the two surface, and d is the separation distance between two surfaces. If the decrease of the van der Waals force is dominant over the increase of the capillary force, the adhesion forces can be reduced by roughening surfaces. Therefore, roughening the surface could be a very useful technique in reducing stiction and adhesion, even for silicon and silicon-related materials. For example, low-adhesion poly-silicon surfaces with a small amount of isolated needle-like asperities have been obtained by etch texturing [18]. If θ_0 is larger than 90° (i.e. hydrophobic surface), the apparent contact angle can be enhanced by increasing surface roughness no matter which kind of liquid–solid contact is formed. Even superhydrophobic surfaces with apparent contact angle larger than 150° can be produced by roughening surface [19–21] or fabricating micropattern surfaces [22]. In this case, the capillary force vanishes; moreover, roughening surfaces can reduce the van der Waals force. Therefore, the rough surface has low adhesion forces and reduced tendency for stiction compared to the smooth surface. Figure 8 gives the water contact angles of polytetrafluoroethylene (PTFE) and micro-scale adhesion force between Si_3N_4 ball and PTFE (the data from Ref. [20]). It can be seen that with the micro-scale

surface roughness increasing, the water contact angle increases, and the micro-scale adhesion force decreases. Many components, such as nature of materials, surface energy, roughness, surface topography as well as surface engineering process, can affect stiction. For the material used in Ref. [20], the micro-scale average roughness above 600 nm appears to minimize stiction due to increasing the water contact angle and decreasing the micro-scale adhesion force. For the fluorocarbon films deposited by DRIE, even a smooth surface with average roughness about 1 nm (determined from $5 \times 5 \mu\text{m}^2$ AFM images) has been shown to have good anti-stiction behaviour in nanoimprinting process [13,23]. In this case, roughness is not a primary contributor to stiction.

5. Conclusion

Stiction is closely related to surface energy of used materials and topography of surfaces. The surface energies and stiction of commonly used MEMS materials have been investigated by contact angle measurements and atomic force microscopy. The five as-deposited/received MEMS materials including silicon, poly-silicon, low-stress silicon nitride, PMMA and SU-8 have similar values for dispersive components of surface energies, while silicon and silicon-related materials have much larger polar components of surface energies than that of PMMA and SU-8, and thereby larger surface energies and enhanced susceptibility for stiction. The nano-scale adhesion force measurements by AFM show that the nano-scale adhesion forces of PMMA and SU-8 are 3–4 times smaller than that of as-received silicon wafer with native oxide. The surface modifications and coatings of silicon can produce a surface with lower surface energy. The wet etching process to remove the sacrificial oxide layer in silicon micromachining could leave an H-terminated surface, which has lower surface energy and adhesion force, and can improve the hydrophobization of single-silicon and poly-silicon although the H-terminated surface is not stable enough for anti-stiction and anti-adhesion applications. The fluorocarbon films deposited by passivation process in deep reactive ion etch could be an efficient solution,

which have the water static contact angle as high as 110° , the surface energies as low as 14.32 mJ/m^2 , and the nano-scale adhesion force as low as 33 nN, which is 4.7 times smaller than that of as-received silicon wafer. The nano-scale adhesion force is closely related to the surface energy of materials. The material surfaces with higher surface energy have higher adhesion force and thereby higher tendency for stiction. For such hydrophilic surfaces as silicon, tendency for stiction could also be reduced by roughening surface due to reduced van der Waals force on the rough surface and contact area. For the hydrophobic rough surfaces, the reduced adhesion force is due to vanished attractive capillary force and reduced van der Waals force. In order to minimize stiction in MEMS fabrication and applications, it is quite important to select suitable materials/processes or give proper surface modifications.

Acknowledgment

We acknowledge financial support from European Commission under contract G1ST-CT-2002-50354.

References

- [1] Tai-Ran Hus, *MEMS & Microsystems: Design and Manufacture* (McGraw-Hill Companies, Inc., New York, 2002).
- [2] R. Ruhmann, K. Pfeiffer, M. Falenski, F. Reuther, R. Engelke and G. Grutzner, *Mstnews* 1 (2002) 45.
- [3] K. Komvopoulos, *J. Adhesion Sci. Technol.* 17 (2003) 477.
- [4] R. Maboudian and R.T. Howe, *J. Vac. Sci. Technol. B* 15 (1997) 1.
- [5] A.W. Adamson and A.P. Gast, *Physical Chemistry of Surfaces* 6 ed. (John Wiley & Sons, Inc, New York, 1997).
- [6] D.K. Owens and R.C. Wendt, *J. Appl. Polym. Sci.* 13 (1969) 1741.
- [7] D.H. Kaelble and K.C. Uy, *J. Adhes.* 2 (1970) 50.
- [8] W. Rabel, *Farbe Lack* 77(10) (1971) 997.
- [9] SU-8 2005 from MicroChem Corp.
- [10] Krüss GmbH DSA I software database.
- [11] B. Bhushan, *Handbook of Micro/Nanotribology* 2 ed. (Chemical Reber Corp, Boca Raton, FL, 1999).
- [12] R. Juan and B. Bhushan, *ASME J. Tribol.* 116 (1994) 378.
- [13] Y.X. Zhuang and A. Menon, *J. Vac. Sci. Technol. A* 23 (2005) 434.
- [14] A.A. Ayon, D.-Z. Chen, R. Khanna, R. Braff, H.H. Sawin and M.A. Schmidt, *Mat. Res. Soc. Symp. Proc.* 605 (2000) 141.
- [15] R.N. Wenzel, *Ind. Eng. Chem.* 28 (1936) 988.
- [16] A.B. Cassie and S. Baxter, *Trans. Faraday Soc.* 40 (1944) 546.
- [17] K. Komvopoulos, *Wear* 200 (1996) 305.
- [18] R.K. Alley, P. Mai, K. Komvopoulos and R.T. Howe, *Proceedings of the Seventh International Conference on Solid-state Sensors and Actuators, Transducer '93*, Yokohama, Japan, Vol. 288, pp. 7–10.
- [19] S. Ren, S. Yang, Y. Zhao, T. Yu and X. Xiao, *Surf. Sci.* 546 (2003) 64.
- [20] E.S. Yoon, S.H. Yang, H. Kong and K.H. Kim, *Tribol. Lett.* 13 (2003) 145.
- [21] S. Shibuichi, T. Onda, N. Satoh and K. Tsujii, *J. Phys. Chem.* 100 (1996) 19512.
- [22] J. Bico, C. Marzolin and D. Quéré, *Europhys. Lett.* 47 (1999) 220.
- [23] D. Nilsson, S. Jensen and A. Menon, *J. Micromech. Microeng.* 13 (2003) S57.

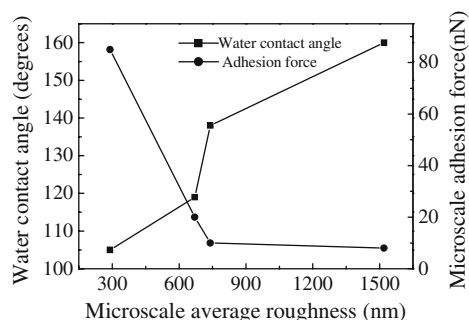


Figure 8. Water contact angle of polytetrafluoroethylene (PTFE) at various micro-scale average roughness (from Ref. [20]).